UC Irvine
UC Irvine Previously Published Works

Title
Electronic Properties of Carbon Nanotubes

Permalink
https://escholarship.org/uc/item/3cg0w2bq

Author
Collins, Philip G

Publication Date
2008

Peer reviewed

eScholarship.org Powered by the California Digital Library
University of California

The Electronic Properties of Carbon Nanotubes

Philip G. Collins[1] and Phaedon Avouris[2]

[1] Department of Physics and Astronomy, University of California, Irvine
Irvine, CA 92697-4576, USA
collinsp@uci.edu

[2] IBM Research Division, T.J. Watson Research Center
Yorktown Heights, NY 10598, USA
avouris@us.ibm.com

This chapter provides a broad overview of the electronic properties of carbon nanotubes, primarily from the point of view of the properties of individual, isolated tubes. The chapter is organized according to the increasing levels of complexity found in nanotube electronics. First, the parent material graphite is briefly introduced, followed by a discussion of the electronic properties of individual, single-walled carbon nanotubes (SWNTs). Next, the experimentally observed properties of both metallic and semiconducting SWNTs are discussed in detail. An introduction to many-body effects and optoelectronic properties of SWNTs is also provided. Towards the end of the chapter, more complex nanotubes and nanotube aggregates are discussed, since these types of samples derive many of their characteristics from SWNT properties. The chapter concludes with a short survey of near-term applications which take advantage of nanotube electronic properties.

I. Introduction

Carbon nanotubes, first observed by Endo (*1, 2*), have attracted a great deal of scientific attention as a unique electronic material. Immediately following Iijima's detailed observations (*3*), theoretical models started appearing predicting unusual electronic properties for this novel class of materials. Unlike other materials known at the time, carbon nanotubes were predicted to be either metals or semiconductors based on the exact arrangement of their carbon atoms (*4, 5*). At that time, the idea of testing such predictions seemed fanciful – imaging these wires required the highest resolution

transmission electron microscopes (TEMs), after all, and researchers joked about nanometer-scale alligator clips making the necessary electrical connections.

The jokes were short-lived, of course, as a number of enabling technologies matured and proliferated throughout the 1990's and ushered in the new "nanoscience" field. Scanned probe microscopes (SPMs) became standard laboratory equipment, field-emission scanning electron microscopes (SEMs) made nanoscale imaging easier than ever before, and electron-beam lithography brought ultrasmall electronic device fabrication to hundreds of university campuses. By taking advantage of the long length of nanotubes, research groups rapidly demonstrated electrical connections to individual nanotubes and a flood of interesting measurements began.

Historically, the first electrical measurements were performed on multi-walled nanotubes (MWNTs) (*6*), nanotubes composed of multiple concentric graphitic shells. However, the electrical characterization of nanotubes began in earnest in 1996, following the distribution of single-walled nanotubes (SWNTs) grown by Andreas Thess in Richard Smalley's group at Rice University (*7*). The simpler, single-walled morphology is more theoretically tractable, and electronic devices composed of SWNTs turn out to be sufficiently complicated without any additional shells of conducting carbon.

II. Semimetallic Graphite

Graphite is a semimetal, a highly unusual electronic material with a unique Fermi surface. As a result, the additional quantization present in nanoscale graphitic fragments is a fascinating subject, resulting in electronic properties which cannot be duplicated by nanowires composed of normal metals or semiconductors.

Graphite has layered structure composed of parallel planes of sp^2-bonded carbon atoms called "graphene" layers. These layers are 0.34 nm apart and only interact via weak, van der Waals forces. The quantum electronic states of a graphene sheet are purely 2D, with nearly continuously varying momenta in the plane (k_x, k_y), but with only a single allowed value for k_z. This 2D confinement does not in itself lead to deviations from the standard Fermi liquid model. A nearly free-electron system in 2D has the same parabolic energy dispersions as a 3D system, though the surfaces of constant energy will be circles or curved lines instead of the more familiar spheres and spheroids.

Figure 1 depicts the 2D bandstructure of a graphene sheet. Many of the constant energy surfaces in graphene are circular lines, but a notably different geometry occurs at the high-symmetry corners k = **K** of the first Brillouin zone. At each corner, two bands[*] cross each other with almost perfectly linear dispersion, and the constant-energy surface shrinks to a discrete point. Quasiparticles on linear bands have no "effective mass" by standard definitions and may be treated with the Dirac equation for massless fermions. Because of the crystal symmetry, exactly six points in k-space exhibit this unusual effect, all having the same magnitude of momentum $|k| = \sqrt{k_x^2 + k_y^2} = \pi / a$, where a is the hexagonal lattice constant of 0.25 nm. While band-edge states are typically immobile standing waves centered on the atomic lattice, the graphene states have a nonzero and nearly energy-independent velocity $v_F = 8 \times 10^5$ m/s.

These unusual features would be easily overlooked if not for the fact that they lie directly at graphene's Fermi energy E_F, the principal energy of interest for nearly all electronic properties. Both carbon atoms in the unit cell contribute one delocalized p_z electron to the crystal, so it is perfectly natural for the p_z-derived band to each be exactly filled to the band edge **K**. This filling sets E_F exactly at the band intersection where the number of available quantum states shrinks to a point. Whereas normal metals might have spherical Fermi surfaces with many available quantum states, graphene has a Fermi "surface" composed of only six allowed momenta — more accurately, the surface is a sparse collection of Fermi points. In can be considered either a very poor metal or a zero-gap semiconductor.

This low number of states accounts for many of the unusual properties in graphene-based materials. 3D graphite is categorized as a semimetal (*8, 9*) and exhibits a relatively high resistivity ρ ~ 10 mΩ-cm, a nonlinear current-voltage dependence, and an unusual cusp in the electronic density of states D(E) at $E=E_F$.

III. Single-Walled Carbon Nanotubes

1. Further Quantization of the Graphene System

[*] The two bands derive from the π states of sp^2-bonded carbon. Two π states, one occupied and one unoccupied, result from having two atoms per unit cell.

The valence and conduction bands of all materials are drawn as continuous but are actually composed of closely spaced, discrete states. These states have a regular separation Δk inversely proportional to L, the macroscopic length of the sample, and for large L (compared to the atomic lattice spacing) the states are effectively continuous. For nanometer-scale materials, Δk can increase to the point where very few k values are allowed and the bands of states become quite sparce. Under these conditions, electrons no longer freely hop from one state to another – the change in either momentum or energy becomes too great for the available thermal fluctuations – and the material is considered to be strongly quantized.

Of course, a sample can be quantized in one of its dimensions and not another. A suitably thin film will retain a continuum of allowed states k_x and k_y in the plane of the film, even if only a few, well-separated wavevectors k_z remain accessible perpendicular to the plane. In a nanowire, one of the wavevectors remains quasi-continuous while the two wavevectors perpendicular to the wire's longitudinal axis become strongly quantized. To visualize the available electronic states for a nanoscale 2D film or 1D wire, it often suffices to extract a plane or a line, respectively, out of the material's 3D bandstructure. For a typical metal or semiconductor, this extra quantization rarely results in dramatic electronic effects: bulk metals tend to produce metallic nanowires, and bulk semiconductors produce semiconducting nanowires, though with possibly modified bandgaps.

Graphene begins as a 2D material, but it too may be further quantized by slicing a narrow strip from the sheet. In this case, the allowed electronic states constitute a line of points, or "band," sliced from the graphene 2D bandstructure. If the width of the strip is *N* atoms, then *N* parallel subbands constitute the complete set of allowed states. Each subband corresponds to a different wavevector in the strip's narrow dimension, analogous to the different transverse modes of a waveguide.

As depicted in Figure 2, it is possible to extract slices from graphene's bandstructure with remarkably different properties. A slice in the direction of a **K** point will include two of the graphene Fermi points and be metallic, but a slice in a different direction may not. Accurately describing a 1D graphene strip therefore requires two independent parameters: both the width of the strip as well as the angle of the strip with

respect to the atomic lattice. Only with both parameters can the electronic properties of the strip be completely specified.

Fundamentally, the SWNT is isoelectronic with this narrow graphene strip with only minor differences. The edges of the narrow strip dictate boundary conditions of a hard-wall potential; the cylindrical SWNT, on the other hand, merely requires single-valuedness around the circumference. This more relaxed boundary condition does not impose any additional energy cost and, as a result, the SWNT's electronic subbands will have almost identical energy dispersions as the parent graphene. In other words, the graphical construction of "slices" from the graphene bandstructure is even more accurate for the SWNT than it is for the flat strip*.

Two constructions of this sort are depicted in Figure 2. It is convenient to specify the circumference of a SWNT as a vector composed of the two primitive lattice vectors, $\vec{c} = n\vec{a}_1 + m\vec{a}_2$. In this scheme, the two parameters specifying the SWNT are the vector indices (n,m) instead of the magnitude of the circumference and an angular orientation. For all SWNTs with n=m, one of the allowed subbands of states runs directly from k = 0 to k = **K**, making all such SWNTs metallic conductors. For SWNTs with n≠m, the subband intersecting k = 0 will not cross the **K** point. Nevertheless, one of the other, parallel subbands may intersect **K**. A geometric construction proves that when the difference between n and m is divisible by 3 (e.g. n – m = 3j, with j = 1,2,3…), one of the various allowed subbands intersects the **K** point and causes the SWNT to be metallic. This leads to the result that 1/3 of all possible carbon SWNTs are metallic and 2/3 are semiconducting. It is believed that the effects of curvature may introduce very small electronic gaps in the metallic SWNTs with n≠m, but these gaps have energies well below room temperature (*10*).

The SWNTs which are not metallic have direct semiconducting bandgaps E_g, the magnitude of which follows a straightforward rule. Because graphene's energy dispersion near E_F is linear in k, the energy gap between the states closest to **K** is directly proportional to the separation Δk between subbands. Δk is itself solely determined by the

---

* An exception occurs when the nanotube is sufficiently small that curvature-induced strain modifies the electronic states. For nanotube diameters of 1.0 nm and larger, these effects can generally be ignored, but smaller nanotubes or nanotubes with mechanical kinks will exhibit rehybridized bonds due to curvature effects.

width of the graphene strip (or of an unrolled SWNT) and the lattice constant *a*. So all SWNTs of a given diameter D will have the same semiconducting bandgap E_g, regardless of the precise values of *n* and *m*, and the value will be E_g = (0.85 eV-nm) / D. Typical experimental SWNT diameters of 1.0, 1.4, and 2.0 nm give optical bandgaps of approximately 0.85 eV, 0.60 eV, and 0.43 eV, respectively.

2. Electronic Properties of Metallic Nanotubes

Metallic SWNTs are those which have a subband intersecting the symmetric Fermi points $k = \pm \mathbf{K}$. Each Fermi point contributes one "forward moving" wavevector with $v_g > 0$ and one "backward moving" wavevector with $v_g < 0$. Including the spin degeneracy there are exactly 4 forward moving electron states and 4 backward moving ones at zero temperature.

Each of these states carries current and, in the absence of any scattering, will contribute one quantum of conductance $G_o = e^2/h = 39\ \mu S$. Elastic scattering may be included in this Landauer model (*11, 12*) as a non-unity transmission coefficient *T*, in which case the total conductance of all four states can be simply stated as

$$G = G_o \sum T_i.$$

An idealized metal SWNT with four parallel, unity-transmission channels will have a conductance of 155 μS or a resistance R = 1/G = 6.5 kΩ. This idealized value is not temperature-dependent.

In a traditional metal, inelastic electron-phonon scattering from acoustic phonons is the dominant limitation to electrical conductivity, and this scattering limits the applicability of the Landauer model above. In SWNTs, however, electron-phonon scattering is strongly suppressed. The 1D electron states of a SWNT can only scatter into a very limited number of empty electronic states and such events require a large momentum transfer (*13*). The resulting suppression produces long inelastic mean free paths $l_{e\text{-}ph}$, on the order of 0.5 μm at room temperature. For submicron-scaled devices, this means that electron-phonon scattering is essentially absent. In order to experimentally measure $l_{e\text{-}ph}$, on the other hand, devices have been fabricated using millimeter-length SWNTs (*14*). As shown in Figure 3, these lengths conclusively demonstrate the diffusive limit of conduction.

Electron-phonon scattering becomes particularly important at high applied bias (high fields). As the SWNT bias V is increased, additional scattering mechanisms turn on and the SWNT resistance increases as shown in Figure 4. This increase is almost perfectly linear in V, so that the device I-V curve has an apparent current saturation at high bias. The experimental result is quite counter-intuitive: not only does a metallic SWNT break Ohm's law, but it also deviates from the stepwise conductance behavior normally associated with quantum wires (*15*). Nevertheless, the behavior is captured by a simple model of optical phonon emission (*16*). The suppression of electron scattering and thermalization by acoustic phonons allows electrons to accumulate energy in an applied electric field. Once the energy of an optical phonon is exceeded (approx 0.18 eV), spontaneous emission can occur. This dissipative mechanism becomes more active proportional to increases in V.

The direct observation of optical phonon emission is rarely observed in metals. Because of the high fields and associated current densities required, most materials will suffer self-heating and electromigration degradation before a clear phonon emission regime can be reached. In SWNTs, on the other hand, quasi-ballistic transport is nearly dissipationless and the covalently bonded carbon atom lattice is impervious to electromigration. SWNTs readily carry currents of 20 μA, corresponding to current densities exceeding 10^8 A/cm^2, without degradation. At these currents, the I-V curve becomes nearly horizontal: the current saturates as all bias increases are efficiently converted to optical phonon emissions. Higher currents can only be reached by suppressing this emission, for example by using extremely short devices. The mean free path for electron-optical phonon scattering in metallic nanotubes has been experimentally measured to be approximately 10 nm (*17, 18*), and devices fabricated on this length scale can carry many times more current.

In experimental SWNT devices, other mechanisms can also play significant roles and result in low-bias conductances much smaller than $4G_o$. Contact resistance plagued early SWNT measurements, limiting measured conductances to 1 – 10% of the theoretical value. Organic residues from solution-deposited SWNTs and polymer residues from lithographic processing were two common contaminants at contact interfaces. Processing improvements have allowed contact resistances to drop

dramatically, with many research groups now using Pd metal to achieve low-resistance contacts to SWNTs (*19*). However, a simplistic model of a metal-metal interface, even one which incorporates the differing metal work functions, does not necessarily capture the complexity of the SWNT electronic contact. Empirically, good contacts can only be obtained using metals with good wetting properties (at least for SWNTs with diameters larger than 1.5 nm) and across interfacial boundaries extending a few hundred nm along the SWNT itself. These characteristics may indicate the difficulty of establishing adiabatic equilibrium between the few quantum states of the SWNT and the large number of bulk states in the connecting electrodes.

Various other elastic scattering mechanisms can also decrease the SWNT conductance G. Point defects, with their associated localized states and high fields, contribute to elastic scattering. And the mere presence of an underlying substrate, with its associated contaminants or trapped charges, presents the SWNT with a modulated potential energy landscape. Both mechanisms reduce the transmission coefficients T_i within the Landauer model and, in the low temperature limit, can induce localization (*20*). An active area of ongoing SWNT research is focused on freely-suspended SWNTs, in which substrate effects can be eliminated.

In addition to decreasing G, these mechanisms make SWNTs sensitive to external electric fields. An applied field, as from a third gate electrode, can move a localized electronic state in and out of resonance with the conduction electrons at E_F and make G gate-dependent. Because of a prevailing conception of SWNTs as being structurally perfect, many researchers have used the presence or absense of transconductance dG/dV_g to identify a SWNT as having a metallic or semiconducting bandstructure. Indeed, the number of current-carrying states in the energy band of a metallic SWNT is not sensitive to small changes in E_F, so metallic SWNTs should normally have $dG/dV_g = 0$. But in the presence of defects, even metallic SWNTs will exhibit transconductance and can be gated to zero conductance at low source-drain bias. Underestimating this mechanism leads to the misattribution of metallic SWNTs as semiconducting. Furthermore, the possibility of defect-induced barriers severely compromises the ability to conclusively identify small-energy bandgaps from three-terminal conductance measurements.

When both contact resistance and elastic scattering are limited, metallic SWNTs can behave like ballistic conductors. In fact, SWNTs today are routinely measured having 6.5 – 15 kΩ resistances. In this limit, delocalized electrons are coherent along the entire length of a SWNT device, especially at low temperatures. Reflections at the SWNT ends result in electronic standing wave oscillations, directly analagous to those in an optical Fabry-Perot cavity. These electronic oscillations have been directly imaged by scanning tunneling microscopy (*21*) and indirectly observed in the two-terminal conductance (*22*), as shown in Figure 5.

3. Electronic Properties of Semiconducting Nanotubes

Two-thirds of all possible SWNTs are expected to have semiconducting bandstructures with direct bandgaps. As with conventional semiconductors, these SWNTs can have majority hole or electron carriers depending on the position of E_F within the bandgap. Unlike bulk semiconductors, however, it is not straightforward to substitutionally dope a SWNT.

Nevertheless, E_F is easily shifted higher or lower in energy by applied electric fields. The entire carrier population resides on the SWNT surface and is exquisitely sensitive to fields – there is little opportunity for effective screening among 1D-confined charges. In the device geometry of a field effect transistor (FET), a nearby, capacitatively-coupled gate electrode is used to reversibly shift the SWNT E_F to different energies. Other sources of electric fields can include adsorbed chemical species and charge modulations on the supporting substrate. These mechanisms will be discussed after a brief introduction to SWNT FET characteristics.

a) Intrinsic semiconducting SWNTs

The field sensitivity of semiconducting SWNTs is the most desirable property of conducting channels in a FET. In fact, enhancing sensitivity and reducing shielding length scales are among the difficulties faced in improving modern CMOS devices*. In the most commonly used, "backgated" SWNT device architecture, degenerately doped Si

* Solutions such as the double-gated FET and finned-channel FET are enabling current performance increases in CMOS devices, but at the cost of complexity.

wafer serves as a supporting substrate and global gate electrode. SWNT circuits are then fabricated on top of a thin, thermally-grown SiO_2 film and gated by the Si through the oxide. Individual devices can be patterned using electron-beam lithography, but the availability of micron-length SWNTs permits the use of optical lithography, and many research groups have demonstrated wafer-scale device fabrication.

Figure 6 depicts typical transport characteristics of an intrinsic, semiconducting SWNT in a backgated FET geometry. The conductance at negative gate voltages V_g is attributed to hole carriers, and the sharp drop in conductance at the gate threshold V_t corresponds to a shifting of E_F higher into the bandap of the SWNT. At still higher V_g, E_F enters the conduction band and electron transport dominates. The conductance change, shown here spanning five orders of magnitude, constitutes the primary attribute of a FET – an electronically controlled switch – and is a key performance metric. One desires a high conductance "On" state and a low conductance "Off" state. Alternately, low conductance in the "On" state limits achievable drive currents and requires high voltages in cascaded devices. High residual conductance in the "Off" state leads to unacceptable quiescent power dissipation.

Additional important device metrics include the width of the transition region, the effective carrier mobility, and a wide range of other performance parameters which are beyond the scope of this review. To summarize briefly, prototype SWNT FETs exhibit performance which is very competitive or exceeds the properties of modern Si technologies (*23*). By improving on the rudimentary architecture shown above, SWNT FETs have been demonstrated with high mobilities and transconductances, low turn-on voltages, and subthreshold slopes near the thermal limit (*23, 24*). Some of the most important of these characteristics will be treated below.

First, however, it must be noted that SWNT FETs behave differently from conventional FETs in fundamental ways. Conventional FET technologies form source and drain electrodes from degenerately doped semiconductors in order to eliminate Schottky barriers at the interfaces of the semiconductor channel. In SWNTs, such materials are unavailable and metal contact electrodes are usually employed, with Schottky barriers forming at the metal-semiconductor interfaces. Fortunately, Schottky barriers are less consequential in a 1D system than in planar geometries. In particular,

the electrostatics of a 1D SWNT contacting a 3D metal electrode allow the depletion widths to vary considerably with applied biases (*25*). Furthermore, interface states do not pin the Fermi level very effectively, the way they do in planar interfaces, because of the lack of screening in 1D. As a result of these differences, SWNT Schottky barriers are quite sensitive to local electric fields and, in general, the switching in a SWNT FET can be attributed to Schottky barrier modulation (*25, 26*).

Much of the literature on SWNT FETs can be fit by a simple model dominated by Schottky barrier switching. Near $V_g = 0$, an intrinsic SWNT will be insulating with a midgap Fermi level E_F. Small, negative V_g values shift E_F towards the valence band, but conduction remains limited by a large-width Schottky barrier. As V_g becomes more negative, the barrier width decreases and hole conductance increases exponentially. The same occurs for electron carriers at positive V_g. When a work-function mismatch is present at the interface, the bands have additional curvature at zero gate which can exponentially favor one carrier type over another. A review of SWNT Schottky barriers has been presented by Heinze et al (*27*).

Some hope exists of preparing low resistance contacts to semiconducting SWNTs using appropriate metals. Materials-related concerns of the semiconductor industry, however, limit the choices of metals which may be used. Using Pd, experiments have demonstrated a decrease in SWNT Schottky barriers for increasing diameters, to the point that large-diameter (e.g. > 2.0 nm) SWNTs exhibit negligible barriers (*28*) as shown in Figure 7. Unfortunately, large-diameter nanotubes also have small bandgaps, which limits the achievable "Off" conductance of a device. Ideally, optimal devices would have nearly perfect, low resistance contacts and also small-diameter SWNTs (e.g. < 1.5 nm) having larger bandgaps.

To further emphasize the consequences of Schottky barriers, consider the device transconductance g and carrier mobility μ. These two parameters are common metrics for comparing conventional FETs and they may be extracted from SWNT device characteristics. The transconductance $g = dI_{SD}/dV_g$ is a measure of the sensitivity of the source-drain current to changes in gate voltage, and this parameter determines the width of the switching transition. In conventional devices, g directly measures the capacitive coupling between the gate electrode and carriers in the transistor channel, but in a quasi-

ballistic, Schottky-barrier FET g is wholly determined by the gate's modification of the barrier width. Therefore, the measured SWNT transconductance of 10-20 μS (*24, 29*) misrepresents the device physics if it is interpreted conventionally. Similarly, the mobility μ is a measure of the conductivity per individual charge carrier, and in conventional FETs it is a measure of the carrier velocity (per unit of applied field). In a quasi-ballistic FET the SWNT mobility is an "effective mobility" in the sense that it does not merely reflect carrier velocity but also the tunneling characteristics of the Schottky barriers. In long SWNTs where the bulk scattering dominates and the transport is diffusive, the mobility has its conventional meaning and values as high as μ ~ 100,000 cm^2/Vs have been reported at low fields and room temperature. Theory predicts a temperature- and diameter-dependence of the low-field mobility (*30*).

The high performance of SWNT FETs is therefore both an opportunity and a challenge, since device development must account for their unusual physics. Already, there is a growing appreciation that these FETs exhibit different scaling rules with respect to channel length and oxide thickness than traditional devices. Novel architectures have demonstrated a variety of performance improvements (*24, 29, 31, 32*), and investigations of high-frequency behavior indicate that SWNTs may operate at competitive switching speeds exceeding 100 GHz.

b) Doping & Chemical Variability in Semiconducting SWNTs

Throughout the early years of silicon transistor research, the presence of unintentional contaminants and dopants complicated and confused experimental efforts. It is not surprising, then, that similar effects have occurred in the SWNT field. Throughout the early literature on SWNT FETs, for example, researchers observed only p-type conduction and no conduction at large, positive V_g (*33, 34*).

Substitutional doping of the SWNTs seemed unlikely, so other mechanisms were proposed to explain this p-type behavior. Ultimately, the SWNT devices were understood to be very sensitive to weakly adsorbed species at or near the Schottky barrier contact, to the extent that simple air exposure was sufficient to cause the apparent SWNT doping. Through a gradual discovery process, a wide range of doping experiments and

theoretical calculations were performed. As a result, the remarkable chemical sensitivity and variability of SWNT circuits is now widely appreciated.

Early doping experiments focused on common graphite intercalants such as iodine and alkali metals, partly in hope of finding superconductivity like in the carbon fullerenes. Instead of superconductivity, though, researchers found irreversible electronic behaviors which seemed strongly dependent on sample history (*35*). The onset of n-type conduction, which might be attributed to alkali metal intercalation, was not reversible in vacuum but immediately disappeared upon exposure to air. Subsequently, it was found that a vacuum treatment alone was sufficient to change the majority carrier type, even in the absence of intentional dopants (*36-39*).

The net result is that SWNT FETs prepared in air will generally exhibit p-type behavior, and that vacuum degassing produces n-type behavior. Using intermediate temperatures, ambipolar behaviors (with E_F near the middle of the semiconducting gap) are also readily obtained. Encapsulation of the devices inside a passivation layer does not interfere with this thermal treatment, so air-stable devices with either carrier type can be selected. The effect is shown in Figure 8 for a sample contacted by Au electrodes, and can be explained in terms of the differing Schottky barrier heights for electron and hole conduction. The work function of Au, like many metals, is very sensitive to molecular adsorbates, and these can raise or lower the effective barriers to carriers in a particular band. The observed p-type behavior is not, therefore, due to hole doping; instead, it arises from a nearly transparent Schottky barrier to holes and an insurmountable one for electrons.

This variability can be considered as either an advantage or a disadvantage for electronic devices. On one hand, the possibility for simultaneous electron and hole injection at opposite ends of a SWNT enables a range of electro-optic behaviors to be described further below. The sensitivity to processing conditions, however, also suggests a variability which poses difficulties for device manufacturing. One solution to this variability is to better match the SWNT's work function with that of the connecting electrodes (*19, 38*). In this case, E_F is most likely to be midgap and neither carrier is preferentially selected by processing. A second solution is to use smaller bandgap SWNTs so that the Schottky barrier effects are minimized (*28*). SWNTs with 2 nm

diameters and even MWNTs are much more likely to exhibit ambipolar conduction than SWNTs with 1 nm diameters. While bandgap reduction can produce low, symmetric Schottky barriers, it also results in high FET "Off" currents. To achieve acceptable, reproducible characteristics, the most effective SWNT devices may ultimately employ a combination of novel architectures, SWNT diameter selectivity, and choice of materials. Figure 9 depicts one such architecture in which the ends of the SWNT are degenerately doped using $SbCl_6^-$ ions to minimize interfacial barriers.

In addition to these Schottky barrier effects, different molecular species have also been observed to shift the turn-on threshold V_T of SWNT FETs. In this case, the effect is similar to traditional doping in which E_F is shifted higher or lower within the bandgap: electron donors increase E_F and lower the necessary V_T for n-type conduction, and electron acceptors do the opposite. This is most strikingly observed for strong oxidants and reducing agents like NO_2 and amines (*40*), but it also occurs for a wide range of reactants including polymers, aromatics, and biomolecules.

The sensitivity of SWNTs is particularly high because these conductors have no shielded bulk atoms. A single monolayer of adsorbed charge donors approaches a 1:1 atomic ratio with the SWNT carbon atoms, allowing for remarkable dopant concentrations. Alternately, charge transfer to the substrate and interfaces can also account for the V_T behaviors observed experimentally. A molecule which chemisorbs to the underlying substrate will produce a local dipole field and partially gate the SWNT. Since SWNTs have no bulk carriers and are not particularly effective at electrostatic shielding, this electrostatic local gating is functionally equivalent to the chemical doping of a particular site. In fact, distinguishing between local electrostatic "doping" and true charge-transfer to a SWNT is experimentally quite difficult. Different chemical species may interact with SWNTs through either mechanism.

It is important to again note that this variability has both positive and negative consequences. Because of the sensitivity of V_T to molecular adsorption, SWNT FETs have been demonstrated as remarkably sensitive chemical sensors. Small, reversible shifts in V_T can lead to orders-of-magnitude change in the FET's source-drain conductance at fixed gate bias. On the other hand, before SWNT FETs may be used as digital logic circuits, this V_T variability must be reliably controlled. Recently, progress

has been made developing air stable dopants that allow even degenerate doping of semiconducting nanotubes and thus make possible new device structures that minimize parasitic capacitances and improve device speed (*24*).

4. Many-Electron Effects in Carbon Nanotubes

Up to this point, the discussion of the ground state electronic structure and electrical properties of carbon nanotubes has been based on a single particle, tight-binding model. While this simple description has been found to be quite successful overall, it fails to explain many important aspects of nanotube behavior.

Ando and co-workers (*41, 42*) discussed the role of e-e Coulomb interactions early on and suggested that they can significantly enlarge the single particle band-gaps in semiconducting nanotubes, a prediction that was later confirmed by first-principles calculations (*43*). The strong e-e interactions, taken in combination with the linear dispersion near E_F in metallic nanotubes, produce a model system for the formation of a state of matter referred to as a Tomonaga-Luttinger liquid (*44, 45*). This state is characterized by unique properties including spin-charge separation and a set of power laws governing current injection through tunneling contacts.

Experimentally, power law dependences of the differential conductance on temperature and voltage have been observed in both bundles (*46*) and individual metallic SWNTs (*47*). Furthermore, the power law exponent was found to depend on the geometry of the contacting electrodes as expected theoretically. The spectral function and the temperature dependence of the intensity at the Fermi level exhibit power law dependences with the appropriate exponents when nanotube aggregates are measured by angle-integrated photoemission (*48*). All of this evidence supports the Luttinger liquid model, though conclusive, direct proof awaits future experiments.

Another inadequacy of the single-particle, tight-binding model is an appropriate description of the excited states of SWNTs. When an electron is promoted to an excited state, an overall attractive interaction develops between it and the hole left behind to form a bound state called an exciton. In a perfect 1D system, the electron-hole (e-h) attraction will be infinite (*49*). While SWNTs are not quite 1D, e-h attraction leads to the formation of strongly bound, quasi-1D excitons. The predicted exciton binding energies range from

~1eV for small diameter (<1 nm), semiconducting SWNTs, to a few tenths of an eV for larger (~2 nm) diameter SWNTs (*50*), with still smaller binding energy excitons occuring even in metallic SWNTs (*50*). Another theoretical prediction is that nearly all of the oscillator strength of the band-to-band transition should be transferred to the exciton, making the inter-band transition nearly invisible to optical absorption experiments (*50*).

Three effects have combined to delay the recognition of these important many-body effects. First, essentially all oscillator strength is concentrated into the excitonic transition so that only one transition is experimentally observed. Second, the strong e-e repulsion is partially cancelled by the attractive e-h interaction, so that experimentally measured excitation energies have reasonably corroborated bandgaps predicted by the simple, single-particle model. Third, the sharp peaks in photoluminescence spectra have been favorably compared to the joint density of states arising from van Hove singularities in the single-particle bandstructure. In fact, these peaks arise from excitonic transitions, not interband transitions. Only recently has two-photon excitation spectroscopy been used to confirm the predicted strong excitonic binding in carbon nanotubes (*51*). The most important implication of many-body effects is therefore that the optical absorption (optical band-gap) does not equal the electrical band-gap in semiconducting nanotubes. This necessitates new types of measurements and the re-interpretation of a number of transport and optical studies.

An outstanding issue which remains to be addressed in future research involves the effect of the SWNT's environment on the above many-body effects. The screening of e-e and e-h interactions is greatly influenced by the dielectric constant of the surrounding environment, since the long-range Coulomb fields are primarily transmitted through the surrounding medium rather than the SWNT body (*50*). Because of this sensitivity, both the electrical and the optical bandgaps become environment-dependent. In fact, any electronic or optoelectronic properties influenced by many-body effects might exhibit environmental sensitivities.

5. Optoelectronic devices

The combination of electronic and optical properties in semiconductor devices comprises a broad and important technological subfield. This section deviates from

strictly electronic properties in order to address the promise of SWNTs for optoelectronic devices. It is a mere introduction to a complex and fast-moving field in which many novel materials have recently attracted attention.

Confined electron and hole carriers can recombine by a variety of different mechanisms. In most cases, the energy will be released as heat (phonon emission), but a fraction of the recombination events can result in the radiative emission of a photon. This process is termed "electroluminescence" and is widely used to produce solid state light sources such as light emitting diodes (LEDs). In order to fabricate LEDs or any other electroluminescent device, one must recombine significant populations of electrons and holes. Conventionally, this is achieved at an interface between a hole-doped and an electron-doped material (e.g. a "p-n junction").

Unlike conventional semiconductors, SWNTs can form ambipolar FETs in which both electrons and holes contribute to the conduction. Using a large source-drain bias, electrons and holes can be simultaneously injected at the opposite ends of a SWNT channel. This allows electroluminescence to occur, as first demonstrated by Misewich et al (*52*). While the emission mechanism is exactly the same as from p-n junctions, ambipolar SWNTs do not require chemical doping and formation of metallurgical interfaces.

Experimentally, SWNT electroluminescence exhibits a variety of interesting properties. The emitted light is strongly polarized along the tube axis. The radiation also has a characteristic energy which depends on the diameter and chirality of the excited SWNT, just as the optical bandgap does. As discussed above, the electronic bandgap is not necessarily the same as the optical bandgap, since the free electron and hole may first form a bound exciton before recombining radiatively. Finally, the geometric length of the electroluminescent region is observed to cover approximately 1 μm. This length may be interpreted as an effective e-h recombination scale, regardless of whether intermediary excitonic binding is first occurring.

Because this recombination length is relatively long, SWNT devices may be fabricated either shorter or longer than it. In short SWNT devices, the light emission encompasses the entire SWNT. In long devices, on the other hand, the emission will be localized wherever the concentrations of electrons and holes overlap most strongly. This

overlap region can be physically moved using a gate electrode, since the relative contributions of electrons and holes to the total current is strongly gate-dependent. As a consequence, a SWNT LED is a moveable light source – an electronic signal V_g can smoothly and continuously position the site of emission (*53*). Figure 10 demonstrates this effect for four different gate voltages. One can immediately envision combining such an LED with an aperture to produce fast electrooptic switches, or electronically moveable light emitters.

In addition to this translatable emission, localized electroluminescence is also observed from particular spots on a SWNT under *unipolar* transport conditions. In this case, the current is exclusively carried by only one type of carrier, but at certain randomly-positioned sites light emission is nevertheless observed. Since both types of carriers are necessary to produce light, these sites must be actively generating e-h pairs. This process could occur, for example, around SWNT defects, trapped charges in the insulator, or any other inhomogeneities which produce large, local electric fields. The monitoring of localized electroluminescence thus provides a potential new tool for detecting defects in SWNT devices or even large-area device arrays.

Photoconductivity is the reverse process of electroluminescence, with optical radiation producing electron and hole carriers. An example of a photoconductivity measurement is shown in Figure 11. The resonant excitation of a SWNT generates measureable electric currents with a reasonable photocurrent yield of approximately 10% (*54*). Alternately, in the open-circuit configuration the SWNT generates a photovoltage, which is then limited in magnitude to the SWNT bandgap (*54*).

Thus, a single SWNT FET device can be used as a transistor, a light emitter, or a light detector. Choosing among these different modes of operation only requires changing the bias conditions and does not require separately tailoring the chemical doping or the device architecture. This flexibility suggests new avenues for SWNT electronics research, since straightfoward fabrications may be able to produce complex, SWNT-based circuitry with both digital logic and optoelectronic capabilities.

IV. Carbon Nanotube Aggregates

1. SWNT Ropes

While individual SWNTs have now been widely studied, much of the preliminary nanotube literature from the 1990's investigated the properties of SWNT "ropes." These agglomerations of SWNTs became widely available for electronics research following the synthesis of Thess et al (*7*). Because the SWNTs had similar diameters, they close-packed like threads in a rope and were even briefly considered to be SWNT crystals. The packing took maximum advantage of van der Waals cohesion and, as a result, made individual SWNTs quite difficult to experimentally isolate.

Even SWNTs of identical diameter have varied electronic properties due to the different possible chiralities. A SWNT rope is therefore most simply modeled as a weakly-interacting bundle of metallic and semiconducting SWNTs in parallel. In reality, the properties of a rope are somewhat more complex. In large-diameter bundles, only a fraction of the SWNTs directly contact the connective electrodes, and metallic SWNTs partially electrostatically shield the semiconducting SWNTs. When the constituent SWNTs are shorter than the rope itself, conduction must be assisted by intertube transport. Moreover, the interstitial sites in SWNT ropes can host a wide range of chemical species. While intercalation may be commercially useful for the storage of methane gas or lithium ions, both intentional and unintentional doping complicated the interpretation of early experimental results.

Despite these numerous obstacles, the availability of SWNT ropes accelerated initial nanotube research. In particular, atomic imaging and spectroscopy by scanning tunneling microscopy (STM) confirmed the field's underpinnings (*55, 56*). Theoretical models were also refined, with SWNT interactions leading to an additional pseudogap in $D(E_F)$ (*10*). However, the synthesis of isolated SWNTs by chemical vapor deposition (CVD) techniques helped overcome many of these materials problems, so that CVD-grown SWNTs were rapidly adopted as an alternative to SWNT ropes.

2. SWNT Films

By spin-coating or spraying a SWNT suspension onto a substrate, macroscopic films of SWNTs may be easily fabricated. The primary advantage of these films is their size, which enabled the earliest attempts to electrically characterize SWNTs. More recently, interest in both thick and dilute SWNT films has seen a resurgence. Thick

SWNT films generally behave like graphitic conductors, albeit with high surface area and mechanical flexibility. As described in the next section, they have shown particular promise as electromechanical actuators (*57*) and as porous electrochemical electrodes (*58*) and commercialization efforts are underway using them as microelectromechanical relays for nonvolatile memory.

Dilute films form percolation networks which, like SWNT ropes, can have complex electronic properties. Of special interest are networks of *sparse* SWNTs, which can be grown using CVD following the dilute dispersal of catalyst particles onto a substrate. This technique produces a loosely connected film composed of semiconducting and metallic SWNTs, each of which retains its individual electronic character. Locally, the electronic properties of such films reflect a parallel combination of the individual SWNTs. Over large areas, however, the films behave as percolation networks dependent on SWNT density and length distributions and on the electronic properties of intertube junctions.

Because semiconducting SWNTs typically outnumber metallic ones by a factor of two, a regime exists above the percolation threshold in which metallic SWNTs do not yet fully interconnect. For films in this regime, every conduction path includes one or more semiconducting segments. These films exhibit remarkably good transistor and chemical sensor behaviors (*59, 60*) considering the presence of metallic components. In practice, the window for fabricating film transistors is not restrictively narrow because SWNT defects and intertube junctions are also sensitive to electric fields. These additional transconductance mechanisms relax the restriction on the metallic number density and have made SWNT film transistors relatively straightforward to fabricate.

Dilute SWNT films have a number of properties which distinguish them from single-SWNT circuits. They do not have the optimum mobility and subthreshold characteristcs of individual SWNTs, but as large-area transistors the films exhibit larger drive currents and have greater tolerance for individual SWNT failures. As demonstrated in Figure 12, they have been incorporated onto plastic substrates as active electronic devices which are both flexible and transparent (*61, 62*). And the element size is well suited for pixellated displays and whole cell biosensors. Thus, while individual SWNT sizes may allow a breakthrough in scaling transistor dimensions downwards, the other

unique properties of SWNTs enable a wider range of electronics opportunities, and research on SWNT films is likely to remain quite active.

3. Multi-walled carbon nanotubes

A multiwalled nanotube (MWNT) consists of individual carbon nanotubes concentrically nested around each other. Unlike the SWNT aggregates described above, MWNTs can have a very high degree of order and three-dimensional crystallinity. Each cylinder, or shell, of the MWNT nests perfectly in the structure with a spacing similar to the interplanar distance in crystalline graphite. Remarkably, however, the electronic communication between these shells is minimal. As in graphite, the physical spacing between layers is 0.34 nm, too large for any significant overlap between the delocalized π orbitals of adjacent layers. Only defects substantially increase the interlayer coupling, and interior MWNT layers are believed to have very low defect densities*.

As a result, the individual layers in a MWNT may be modeled as parallel, independent SWNTs with the properties described above. A rich literature exists on the possible corrections to this simple model, but to first order it is accurate. Nevertheless, MWNTs are exceptionally complex wires. The nesting imposes tight restrictions on the diameter of a particular shell but not on its chirality. Each shell will therefore randomly alternate between semiconducting and metallic (*63*), producing something like a coaxial cable but with many more alternating layers. This effect is shown in Figure 13. The diameter-dependence of SWNT bandgaps is believed to be preserved, so that in the absence of metallic chiralities MWNTs exhibit a radial bandgap variation from shell to shell. A typical MWNT might have shell diameters ranging from 2 to 20 nm, corresponding to electronic bandgaps of 0.3 eV at the inner diameter and 0.03 eV at the outer surface. At room temperature, therefore, the outer shells of a MWNT conduct regardless of chirality, since thermal excitations exceed the small bandgaps (i.e. $kT > E_g$).

A second electronic complication in MWNTs is the existance of closely-spaced electronic subbands above and below E_g. As depicted in Fig. 2, these subbands have

---

* Graphite crystals invariably incorporate line and point defects which account for almost all of the c-axis thermal and electrical conductivity, as well as the sample-to-sample variation in these properties.

energy spacings of the order of E_g. In SWNTs, E_g is sufficiently large that the subbands only play a role in optical properties. In MWNTs, on the other hand, these subbands are merely 10's of meV apart, so that multiple subbands may be thermally populated at room temperature. Furthermore, small amounts of chemical doping (*64*) can shift E_F and ensure that it crosses multiple subbands.

A final complication for MWNT devices is the proper description of their electrical contacts. For a pristine MWNT physically connnected to a metal electrode, only the outermost carbon shell is truly connected in an electrical sense. Inner shells are not ohmically connected but may communicate via tunneling, coulomb drag, diffusive scattering, and a range of other mechanisms. At low temperatures and low bias, these mechanisms can be minimized and the measured conductance will be exclusively due to the properties of the outermost shell. Under these conditions, MWNTs behave very much like large-diameter SWNTs, with quasi-ballistic conduction, coulomb blockade charging effects, and even Ahronov-Bohm-like interferences from circumferential states (*65, 66*).

At high bias, on the other hand, electron injection at the contacts helps to equilibriate multiple shells, all of which contribute to conduction with one or more subbands. Room temperature measurements clearly indicate the contributions of multiple shells, even in the low bias limit (*67*). For example, a MWNT composed of an outer semiconducting shell and an inner metallic shell can be partially gated by electrostatic fields, but never turned off because of leakage through the metallic component. More complete characterizations can individually measure every shell's contribution and sensitivity to electrostatic gating (*63*). Despite this facility, the precise behavior of a given MWNT is difficult to generalize because of the many different types of variability.

Under exceptional conditions, MWNTs can exhibit conductance quantization, even at room temperature. A series of experiments performed with suspended MWNTs dipped into liquid mercury contacts has demonstrated characteristics of single-shell ballistic transport (*68, 69*). These effects are not observed in planar, lithographically-fabricated devices, however, even ones in which the MWNT is suspended across an air or vacuum gap. It may be that unique properties of mercury, combined with a special

preparation which eliminates surface scattering, allows the quantization steps to be observed.

To take full advantage of their inner carbon shells, it is possible to modify a MWNT in various ways. By chemically etching the ends, all of the MWNT shells can be exposed and a metal electrode will then contact each one, albiet with a vanishingly small contact area. Alternately, energetic beams of electrons or atoms can be used to introduce defects and electrically crosslink the shells (*70*). At very low dosages, MWNTs become better conductors due to the contributions of multiple inner shells, but generally the simultaneous loss of crystallinity degrades the conductivity and introduces disorder scattering. Such samples then exhibit unusual bias- and temperature-dependences.

4. Disorder in the Nanotube Nomenclature

Because of the rapidly growing literature on nanotube electronics, it is important to point out that variations exist in carbon nanotube nomenclature. A wide variety of material morphologies exist, especially given the large number of research groups investigating nanotube synthesis. The electronic properties described above are unique to isolated, sp^2-bonded planes of graphitic carbon and do not necessarily apply to more disordered carbonaceous materials.

Two particularly subtle errors frequently mislead researchers unfamiliar with the historical development of the field. First, a wide range of hollow-core materials have been called MWNTs. The earliest MWNTs were grown at very high temperatures in arc furnaces designed for the production and study of fullerenes. High temperatures assist the annealing of sp^2-bonded networks and much of the structural carbon in these nanotubes was believed to be defect-free, making the graphene bandstructure relevant. In such materials, the intershell coupling is indeed minimized and the individual shells can be quasi-ballistic. Theoretical models of MWNTs exclusively refer to such materials. Experimentally, less crystalline carbon wires such as those synthesized at lower temperatures can be highly defective and rarely consist of perfectly nested shells, much less electronically independent ones. These materials generally have the electronic properties of graphitized carbon fibers, which cannot be reasonably compared to the single-conducting-shell results (*65, 68*) described above. A wide range of hollow carbon

wires are called MWNTs only by convenience, even though they may clearly lack the mechanical, chemical, and electronic properties associated with SWNTs and the MWNTs of theoretical models.

A second comment regards the existing literature on SWNTs. The early synthesis of SWNTs was achieved by incorporating transition metal catalysts into carbon plasmas. During the popularization of CVD synthesis, it was therefore widely accepted that catalyst-promoted nanotube growth resulted in SWNTs. Many experimental results have been attributed to SWNTs without any structural characterization other than a measurement of the outer diameter. Subsequently, careful microscopy (*71*) and shell-counting experiments have determined that diameter is a very poor predictor of the number of shells in a CVD-grown nanotube, especially for diameters larger than 2 nm. True SWNTs with diameters of 1 nm, 2 nm, 3 nm, and higher have indeed been observed by high resolution microscopy, but double-walled and triple-walled nanotubes are far more common at the larger diameters and accurate wall counting requires patience and skill. The unintentional experimental confusion on this issue indicates the lack of techniques originally available for characterizing nanotubes integrated into electronic circuits. Today, techniques such as Raman spectroscopy can clearly distinguish between circuits have single-walled or double-walled nanotubes.

V. Electronic Applications of Carbon Nanotubes

Because nanotubes exhibit many interesting electronic properties, a wide range of electronic applications have been proposed and investigated. Various prototype devices have been demonstrated with excellent, commercially-competitive properties.

However, a primary obstacle to many applications remains the variability in electronic characteristics. Chiral variability is a widely acknowledged problem with SWNTs, but there is hope that it may be solved through specially designed catalysts or selective wet chemistry (*72*). An equally serious but less well-documented problem is the sensitivity of SWNTs to small chemical, mechanical, and electronic variations present on substrates, at metal electrodes, and in the SWNTs themselves. Researchers who have produced 4" and 6" wafers full of SWNT devices have sidestepped the chirality problem by manually selecting the subgroups of semiconducting or metallic SWNTs. Even

among these subgroups, electrical properties vary by an *order of magnitude* from device to device, perhaps due to surface contaminants or nanoscale geometric variations. When the SWNT diameter is not precisely controlled, the variations are even larger.

Thus, even if the chirality issue were immediately resolved, consistent specifications for nanotube circuitry would remain elusive. SWNT transistors and memory elements for digital logic can be individually demonstrated but not yet manufactured, and many additional processing techniques remain to be discovered and developed before SWNT devices will have reliable data sheets. In this sense, nanotube electronics resembles early Si research of the 1950's and 60's. Variability remains a primary challenge for nanoelectronics applications in which SWNTs assist downscaling to ultrasmall or ultradense circuitry.

Larger circuits and devices incorporating many nanotubes can be much less sensitive to small fluctuations on individual SWNTs. For example, the thin-film SWNT FETs described above are not particularly small, but their flexibility, reasonable performance, and low-cost fabrication suggest particular application niches. Similar electronic devices which rely only on nanotube ensemble properties can be produced more dependably than single-nanotube devices, and some of these are closer to successful commercialization. The remainder of this section provides a short tour of potential applications enabled by the electronic properties of nanotube ensembles. One must consider, however, whether the performance of these large nanotube ensembles is distinguishable from that of films of carbon fibers, a more traditional and much lower cost material.

1. Conductive Composites

Because of their extreme aspect ratios, nanotubes can form conductive percolation networks at very small volume fractions. By embedding nanotubes into a polymer matrix, antistatic and electrically conductive plastics are readily produced. In fact, such products are the earliest-known commercial applications of carbon nanotubes. The volume fraction of nanotubes can be as small as 0.1% (*73*), allowing the intrinsic properties of the matrix, which might include transparency, flexibility, and strength, to be

retained. At still higher densities, the nanotubes can also begin to tailor the matrix's mechanical properties.

When not confined within a matrix, conductive nanotube films exhibit large surface areas and significant mechanical flexibility. These properties enable electrochemical and electromechanical applications (*74*). For example, nanotube "supercapacitors" exhibit very large capacitances for their size, because even a compressed nanotube film remains porous to most electrolytes. A nanotube electrode with a macroscopic area A has an effective surface area hundreds of times larger than A and exhibits capacitances exceeding 100 Farads per gram of nanotube material (*74*). Furthermore, nanotube supercapacitors can charge and discharge at power rates of 20 – 30 W per gram, sufficient for high power applications such as hybrid-electric vehicles (*75*). The chemical inertness of nanotubes is critical to this type of application: nanotubes do not readily degrade with repeated cycling the way that other high-surface-area materials do. Of course, some electrolytes are more chemically active than others, and the application of nanotubes to lithium ion storage has been hampered by large, irreversible capacitances (*76*). Nevertheless, nearly all lithium ion batteries manufactured today include a small percentage of lifetime-enhancing carbon nanotubes. Both capacitative and chemical energy storage using nanotube electrodes remain active research topics, with products successfully deployed in both areas. However, these applications are quite sensitive to the high costs of nanotube materials and will benefit from ongoing research in bulk nanotube synthesis.

Nanotube films have also been investigated as electronically-controlled mechanical actuators and switching elements. In an electrolyte, the capacitive charging of a nanotube film leads to swelling and mechanical deformation (*57*), which can be employed as a type of actuator. In air or vacuum, electrostatics alone are sufficient to deform nanotubes (*77*), since despite their high tensile strength nanotubes are relatively floppy and bendable. The deformation of individual nanotubes has been imaged by SEM and TEM, and using high frequency fields a nanotube's mechanical resonances can be directly measured (*78, 79*).

Visionaries imagine mechanical work at the nanoscale being accomplished by nanotube actuators and positioners. In the shorter term, electromechanical actuation has

been employed to build simpler electronic switches (*80*). These devices resemble relays with nanotube films as the flexible armature contact. Unlike relays, these mechanical switches do not require magnetic fields or power-hungry solenoids, so they can be lithographically fabricated in large arrays and potentially used for nonvolatile memory applications.

2. Electron Emitters

As chemically inert wires with high aspect ratios, carbon nanotubes exhibit all of the properties desired in a good field emitter (*81*). Both SWNTs and MWNTs exhibit emission at low threshold electric fields of 1 to 2 V/μm, indicating that their sharp tips geometrically enhance local electric fields by factors of 1000 or more. The tolerance of nanotubes for extraordinary current densities further allows these emitters to operate at high power densities.

Individual field emitters constitute a small commercial market, but arrays of emitters can be used for general lighting, flat panel displays, and high power electronics. In each of these applications, the nanotube emission exceeds the minimum performance specifications to be competitive; the primary barriers to commercialization involve other issues such as fabrication, compatibility, and product complexity. In lighting, these barriers are relatively small and high-brightness, high-efficiency lighting products exist. Alternately, flat panel displays are highly complex products with interrelated technical, economic, and practical specifications. Display technologies demand thousands of identical pixels, a stringent requirement on emitter variability. In this field, multiple demonstration prototypes by companies including Samsung and Motorola have not yet resulted in consumer products.

Field emission is intrinsically a nondissipative, energy-efficient tunneling process. Emission devices are therefore useful in a variety of high power density applications, such as the frequency modulation of very large currents or surge protection for power and telecommunications substations. In the past, potential power devices such as these have been severely limited by the available field emission materials, and nanotubes have made new performance levels possible.

Additionally, a field emission beam is very energetic, and when directed at a metal target it can generate x-rays (*82*). Before nanotubes, field emission sources lacked the current densities necessary to produce high flux x-ray sources for medical imaging or scientific equipment. As a result, x-ray equipment has depended on power-hungry, water-cooled, thermal electron sources. The advent of nanotube-based x-ray sources allows low weight, low power, portable devices, with the added advantage of higher spatial resolution and longer lifetimes compared to thermal sources (*82*). These devices are currently being developed for multiple applications including biomedical scanning, airport security, and space exploration, as depicted in Figure 14.

3. Chemical and Biological Sensors

Chemical and biological sensing constitute a broad market fragmented into many niches and served by a wide variety of transduction mechanisms – optical, electrochemical, mechanical, and electronic. Electronic sensors have generally competed poorly because of the difficulty of interfacing solid state circuits with chemically-specific functional molecules, and doing so without inducing temperature, humidity, and temporal variabilities.

In principle, SWNTs are ideal for electronic chemical sensors. Charge carriers are exclusively confined to the conductor's surface and the measured resistance can be sensitive to individual scattering sites. Even though applications requiring large numbers of identical FETs remain out of reach for SWNT electronics, a chemical sensor demands only a few individual circuits. Put another way, a chemical sensor can exploit one of the biggest weaknesses of SWNT circuits, namely their sensitivity to chemical perturbations. Nevertheless, the very possibility of chemical sensitivity was not appreciated in the early years of SWNT research. Attempts to intentionally dope individual SWNTs led researchers to uncover unexpected sensitivities to air exposure and re-evalaute the p-type behavior of SWNT FETs (*36*). Subsequent experiments found sensitivities spanning from reagents like NH_3 and NO_2 (*40*) to inert gases (*83*).

The field of chemical sensing continues to be unique among the electronic applications described here because it remains poorly understood on a fundamental level. No single explanation can account for all of the experimental evidence of chemical

sensitivity in SWNT circuits. Active hypotheses include chemical doping of SWNTs by charge transfer, electrostatic doping via charge transfer to the supporting substrate, modulation of interfacial (Schottky) barriers due to adsorption on the metal electrodes, chemical modification of defect sites, mechanical impingement and deformation of the SWNT structure, and simple van der Waals interactions.

Nevertheless, the development of SWNT chemical sensors is progressing remarkably quickly considering that so little has been confirmed regarding the transduction mechanisms. Experimentalists have confirmed the effect, tailored its usefulness, and sensor products are now commercially available. Prototype sensors exist which can test for dilute toxic gases, hydrogen gas leaks, traces of explosives, and specific analytes in medical patients' breath. By extending the principle to SWNT devices coated with proteins or antibodies, simple biochemical sensors have also been demonstrated (*84*). Similar progress with a variety of non-carbon nanowires provide researchers significant latitude to choose an appropriate surface chemistry for a particular analyte. The carbon SWNT, however, may provide an optimum starting point for leveraging organic chemistry. Direct linkages of carbon SWNT circuits into biomolecular processes is a new research opportunity which is only beginning to be explored, and the field is likely to grow rapidly in coming years. The concept captures the broad premise of nanotechnology and suggests that the highest impact applications of SWNT electronics may result from innovation at the boundaries between solid state electronics, chemistry, and life sciences.

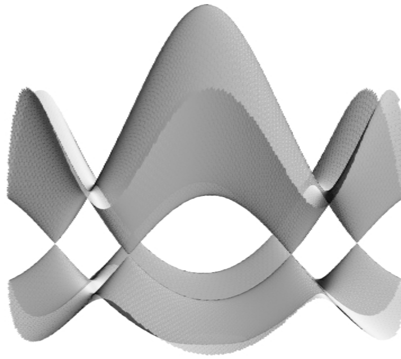

Figure 1. The electronic bandstructure of a graphene sheet has band crossings at the high-symmetry corners **K** and **K'** of the Brillouin zone. The Fermi level E_F intersects these crossings, resulting in the semimetallic properties of graphene and graphite.

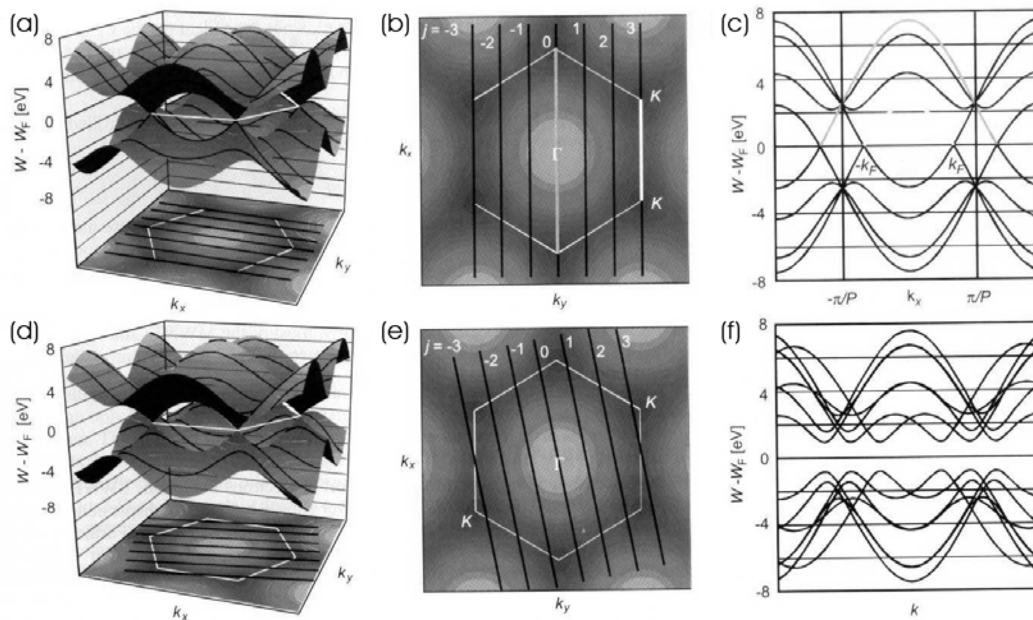

Figure 2. 1D quantization of the graphene bandstructure for different nanotube symmetries. The top row corresponds to an "armchair" nanotube in which a subband directly intersects the **K** symmetry points (a,b) and results in a metallic bandstructure (c). In the bottom row, a chrial nanotube's subbands miss all of the **K** points (d,e) and the bandstructure is semiconducting. Reproduced from Dresselhaus et al. (*85*).

Figure 3. SWNT resistance versus device length. At very short lengths, a metallic SWNT is quasi-ballistic and the device resistance can approach the fundamental minimum of 6.5 kΩ. As device lengths exceed the mean free path for acoustic-phonon scattering, the resistance becomes diffusive with a resistivity of approximately 6 kΩ/µm. Reproduced from Li et al. (*14*)

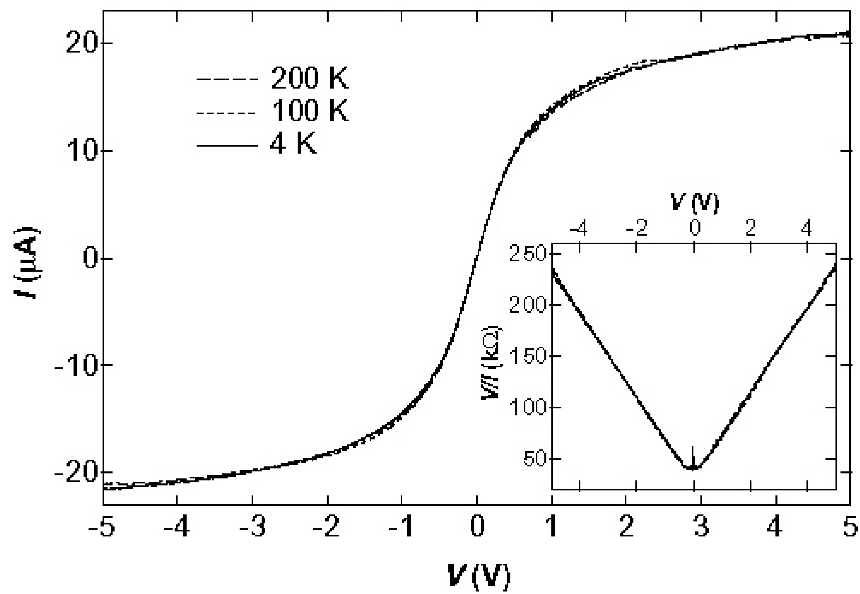

Figure 4. SWNT current and resistance (inset) versus applied bias V. Over a wide bias range, the resistance increases linearly with V and is relatively insensitive to temperature. The behavior matches a model in which low-energy, acoustic phonon scattering is nearly absent and the resistance is predominantly due to high-energy, optical phonon emission. Note that this device, which is approximately 1 μm in length, has a small but non-negligible contact resistance. Reproduced from Yao et al. (*16*)

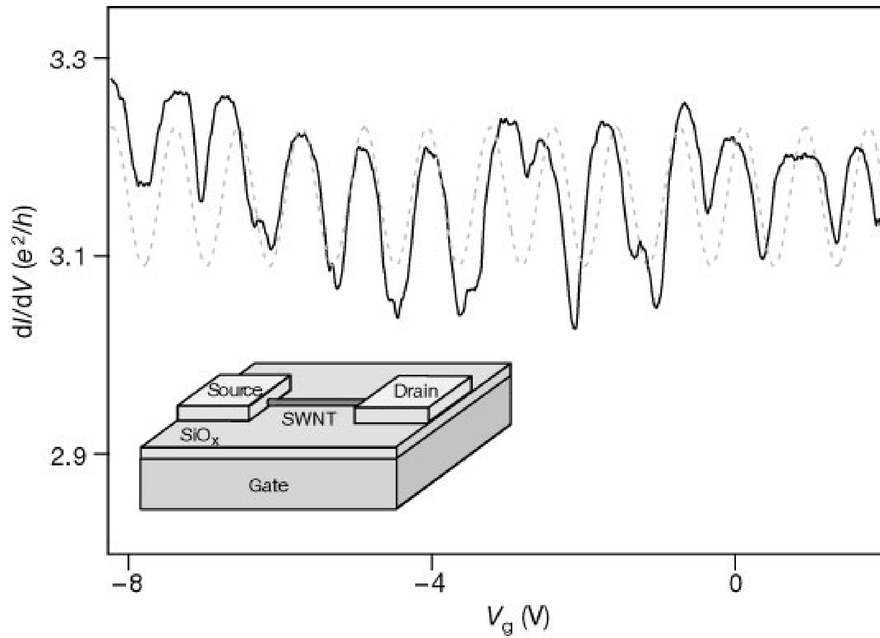

Figure 5. Differential conductance of a metallic SWNT 200nm in length. With sufficiently good contacts, the SWNT conductance approaches the theoretical limit of $4e^2/h$. The periodic oscillations with gate bias V_g correspond to Fabry-Perot interferences of electrons reflecting off the source and drain electrodes. This measurement is performed at T = 4K. From Wenjie et al. (*22*)

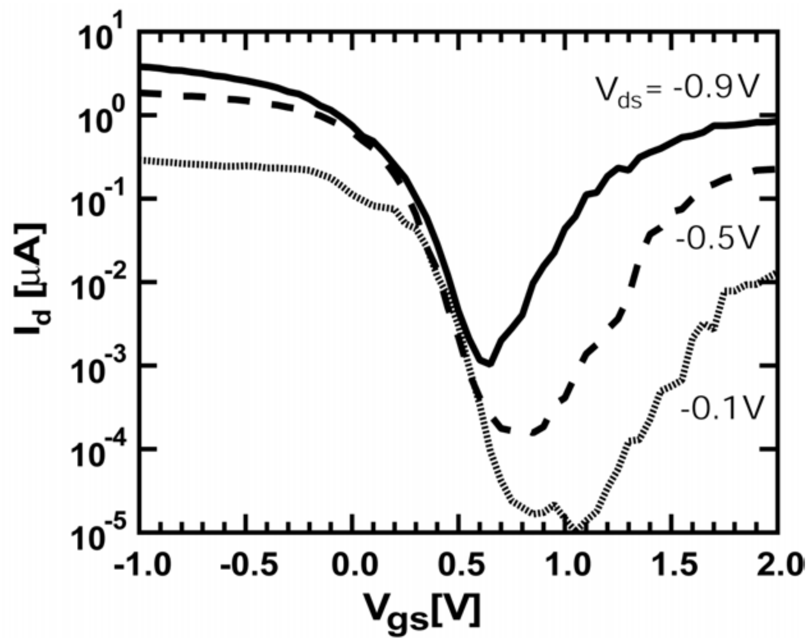

Figure 6. Gate dependence of an ambipolar SWNT FET. At positive gate bias, the conductance is primarily due to electron carriers, while at negative gate the carriers are holes. Near the threshold voltage, the Schottky barriers for holes and electrons are approximately equal and both carriers can be injected when the source-drain bias is large. Alternately, small biases maximize the achievable on-off ratio. From Y-M. Lin et al. *(86)*.

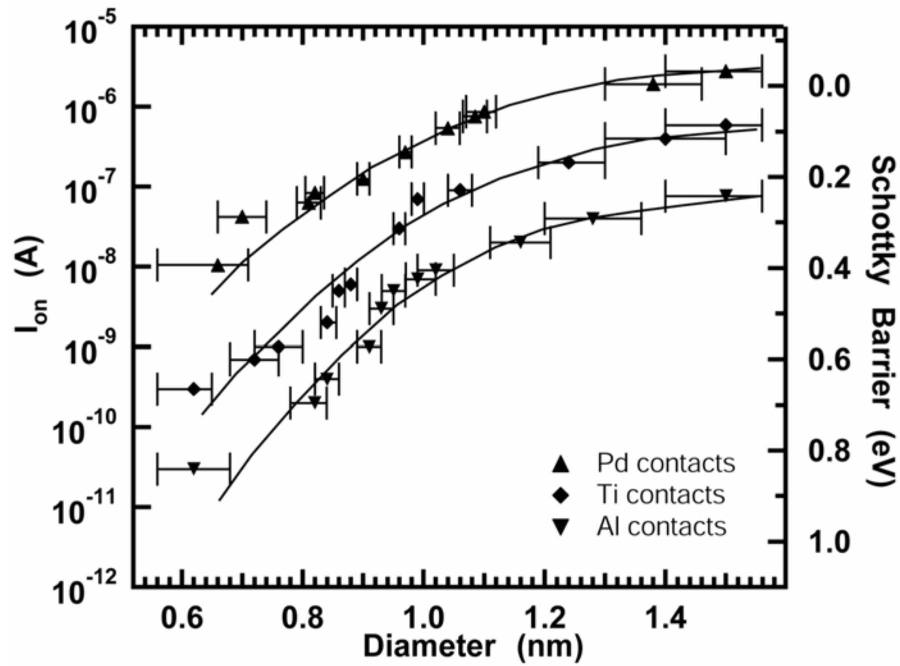

Figure 7. Schottky barrier contacts limit the maximum possible drive current in a SWNT FET. The barrier height is sensitive to both the SWNT diameter and the contact metal. For low work function metals like Pd contacting small gap (large diameter) SWNTs, the effective barrier is minimized and maximum currents are achieved. The data points shown here are measured with a 0.5V source-drain bias at a gate voltage $V_g - V_T = -0.5V$. From Chen et al. (*28*).

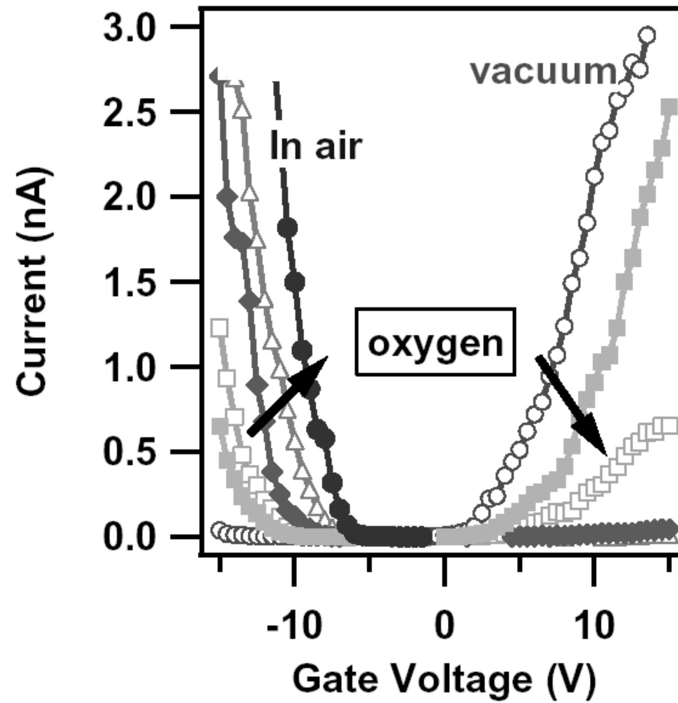

Figure 8. The apparent majority carrier in SWNT FETs changes from electrons in air to holes in vacuum, with a strong dependence on the presence of oxygen. This effect is due to a shift in the work function of the connective Au electrodes. In air, the work function mismatch to the SWNT results in a smaller Schottky barrier for holes than for electrons. In vacuum, the Au work function increases and the reverse becomes true. From Derycke et al. (*39*).

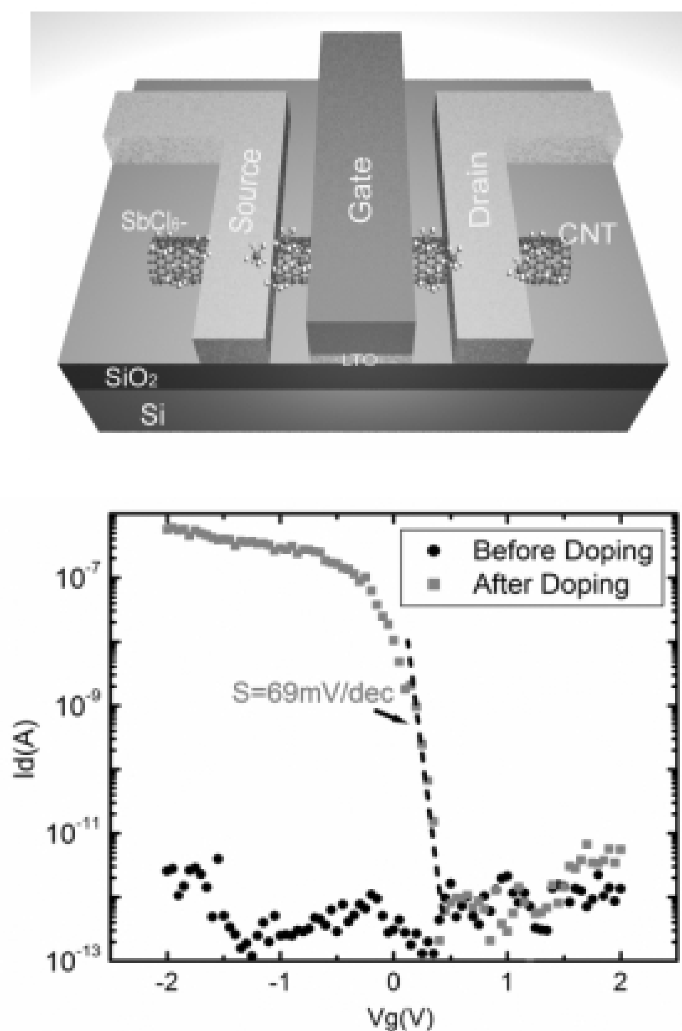

Figure 9. In traditional semiconductor devices, degenerately doped semiconductors form the source and drain contacts to the semiconducting channel. Similar effects in SWNT FETs can minimize Schottky barrier effects. Here, a partly-exposed SWNT is oxidized by $SbCl_6^-$ ions in order to degenerately dope the portions which contact the source and drain electrodes. The resulting FET characteristics exhibit a sharp conductance transition and very small subthreshold swing S, both of which may be attributed to switching by the SWNT body. From Chen et al. (*24*).

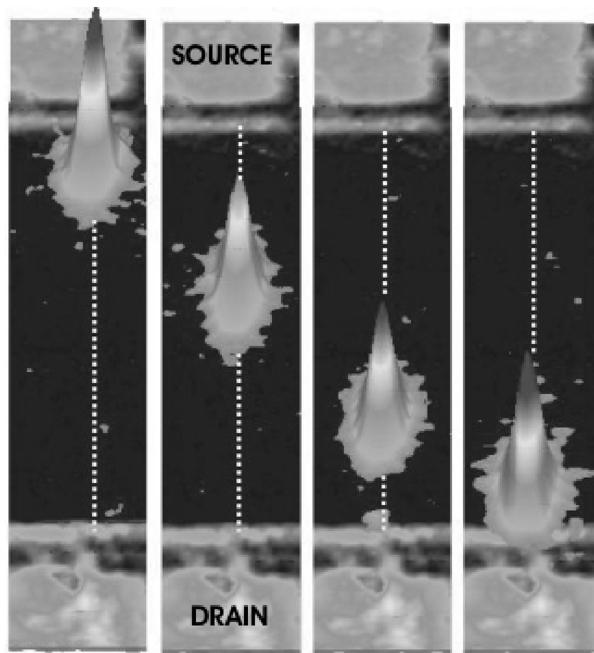

Figure 10. Electroluminescence from a long, single SWNT in a FET configuration. The electron-hole recombination length is short (~ 1 μm) compared to the length of the device, so the point of highest luminescence is easily resolved within the electrodes. Furthermore, this site can be controlled by varying the gate voltage V_g. This figure depicts the luminescence at four different values of V_g. From Freitag et al. (*53*).

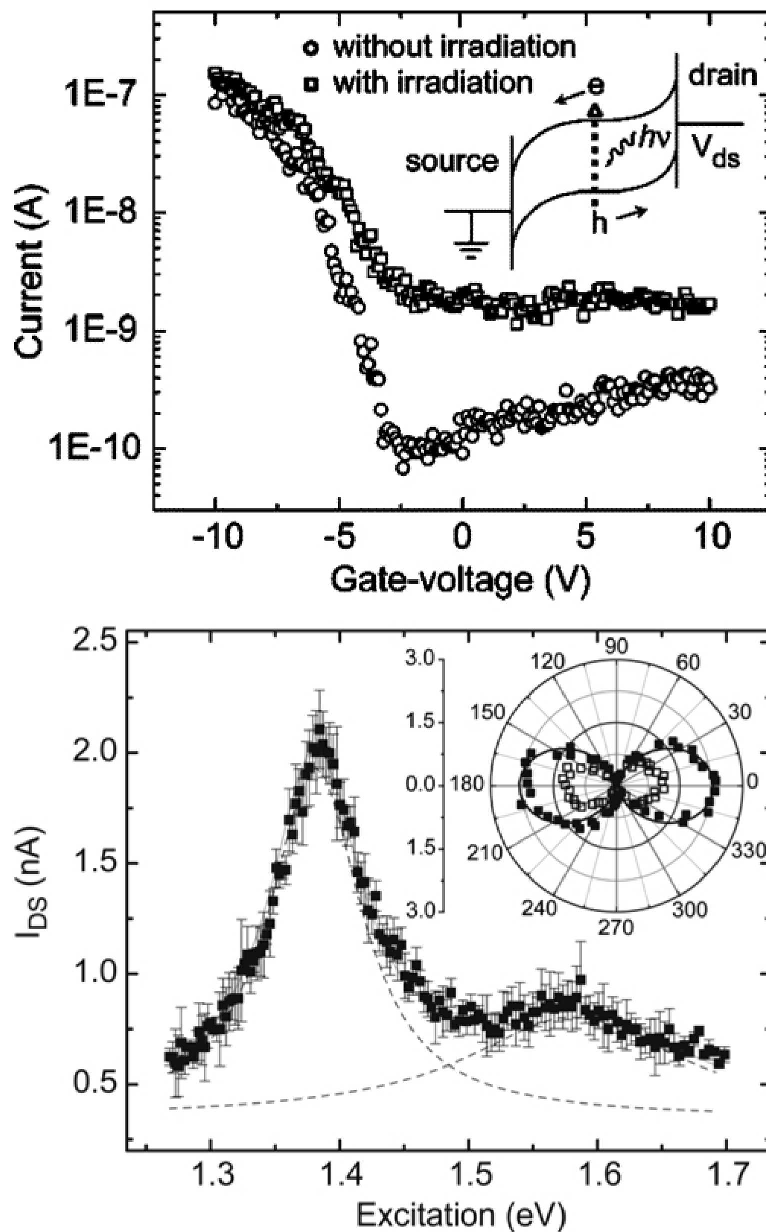

Figure 11. Photoconductivity from an individual SWNT in a FET configuration. Incident radiation produces a large increase in conductivity if it is resonantly tuned to form electron-hole pairs (top). The effect is sensitive to both photon energy (bottom) and polarization (bottom, inset), with polarizations parallel to the SWNT generating the largest photocurrents. The primary resonance near 1.4 eV is due to the creation of excitons (the "E_{22}" transition), and the higher energy peak is a sideband attributed to exciton-phonon coupling. Adapted from Qiu et al. (*87*)

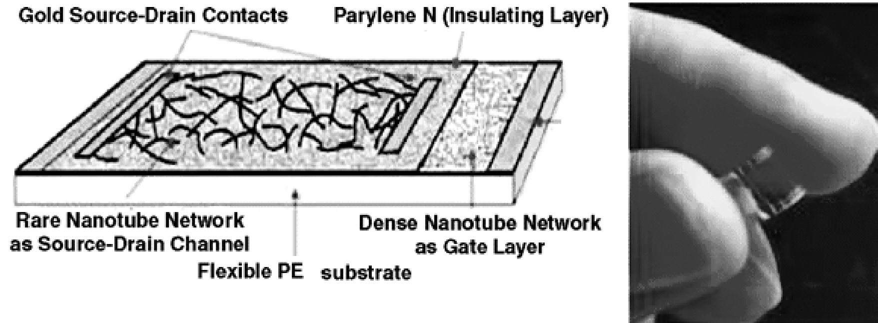

Figure 12. A film of nanotubes on a flexible, transparent substrate can be used as a field-effect transistor. Similar technologies may enable large area flat panel displays or low cost, printable active circuits. From Artukovic et al. (*62*)

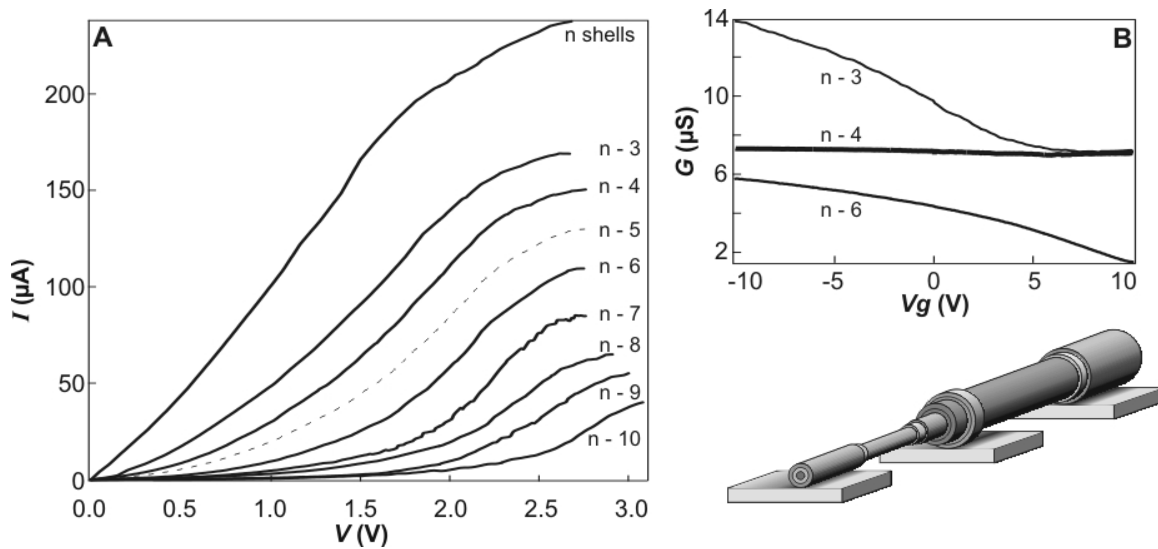

Figure 13. A crystalline MWNT is composed of many nested SWNTs. By peeling away one carbon layer at a time, characteristics of different inner shells may be investigated. Here, the current-voltage characteristics (A) and gate dependence of the conductance (B) are both measured on different layers of a MWNT. Adapted from Collins et al. (*63*).

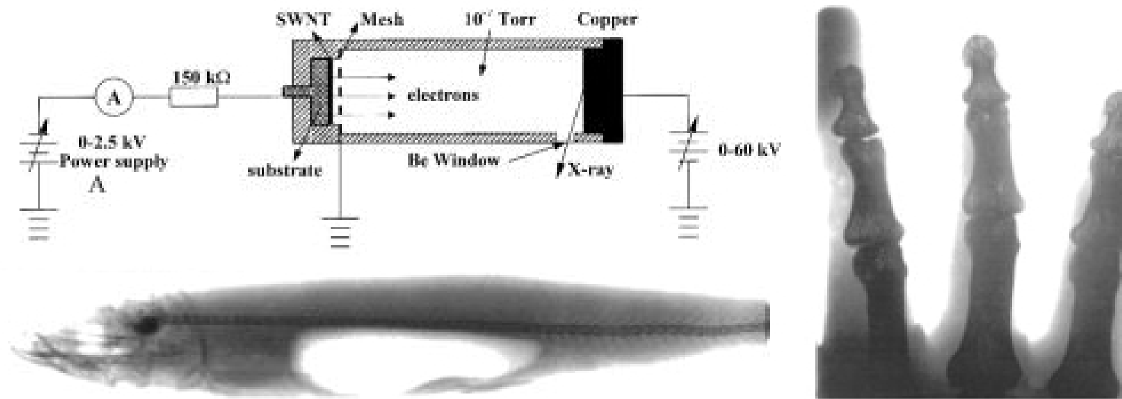

Figure 14. A SWNT cathode is a very effective field emitter, with turn-on fields as low as 1V/μm. The emitted electron beam can be used to light a phosphor or, as shown here, to generate X-rays medical imaging. Adapted from Yue et al (*82*).

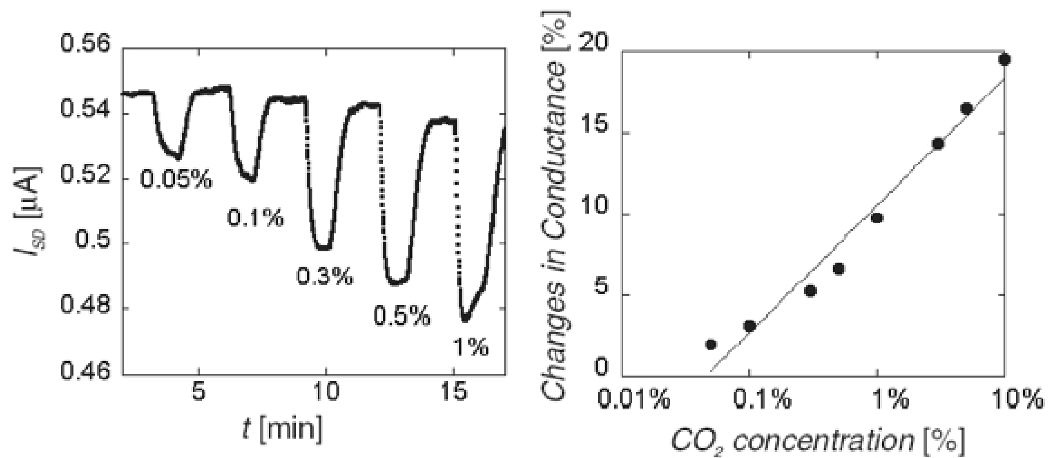

Figure 15. The chemical sensitivity of SWNT FETs may be directed towards different analytes by coating or chemically functionalizing the devices in different ways. Using this approach, sensors selective to various gases and liquids have been demonstrated. Here, a starch-based polymer coating makes an n-type SWNT device sensitive to different concentrations of CO_2 gas. The measurement at left is performed under fixed bias conditions (V_g = +6, V_{SD} = 0.2V). Similar devices are under development for capnography, the monitoring of patient respiration, in which the desired dynamic range is the 0 to 10% CO_2 range. Adapted from Star et al (*88*).

References

1. A. Oberlin, M. Endo, T. Koyama, *J. of Crystal Growth* **32**, 335 (1976).
2. M. Endo, *Chem Tech* **18**, 568 (1988).
3. S. Iijima, *Nature* **354**, 56 (1991).
4. R. Saito, G. Dresselhaus, M. S. Dresselhaus, *Physical Review B (Condensed Matter)* **50**, 14698 (1994).
5. N. Hamada, S. Sawada, A. Oshiyama, *Phys. Rev. Lett.* **68**, 1579 (1992).
6. L. Langer *et al.*, *Journal of Materials Research* **9**, 927 (1994).
7. A. Thess *et al.*, *Science* **273**, 483 (1996).
8. B. T. Kelly, *Physics of graphite* (Applied Science, London ; Englewood, N.J., 1981).
9. K. S. Novoselov *et al.*, *Science* **306**, 666 (2004).
10. P. Delaney, H. J. Choi, J. Ihm, S. G. Louie, M. L. Cohen, *Nature* **391**, 466 (1998).
11. Y. Imry, R. Landaur, *Rev. Mod. Phys* **71**, S306 (1999).
12. S. Datta, *Electronic Transport in Mesoscopic Systems* (Cambridge University Press, Cambridge, 1995).
13. P. L. McEuen, M. Bockrath, D. H. Cobden, Y. G. Yoon, S. G. Louie, *Phys. Rev. Lett.* **83**, 5098 (1999).
14. S. D. Li, Z. Yu, C. Rutherglen, P. J. Burke, *Nano Lett.* **4**, 2003 (2004).
15. B. J. v. Wees, *Phys. Rev. Lett.* **60**, 848 (1988).
16. Z. Yao, C. L. Kane, C. Dekker, *Physical Review Letters* **84**, 2941 (2000).
17. A. Javey *et al.*, *Physical Review Letters* **92** (2004).
18. J. Y. Park *et al.*, *Nano Letters* **4**, 517 (2004).
19. D. Mann, A. Javey, J. Kong, Q. Wang, H. J. Dai, *Nano Lett.* **3**, 1541 (2003).
20. S. J. Tans, C. Dekker, *Nature* **404**, 834 (2000).
21. L. C. Venema *et al.*, *Science* **283**, 52 (1999).
22. L. Wenjie *et al.*, *Nature* **411**, 665 (2001).
23. P. Avouris, M. Radosavljevic, S. J. Wind, in *Applied Physics of Carbon Nanotubes* S. V. Rotkin, S. Subramoney, Eds. (Springer, Berlin, 2005).
24. J. Chen, C. Klinke, A. Afzali, P. Avouris, *Applied Physics Letters* **86** (2005).
25. S. Heinze, M. Radosavljevic, J. Tersoff, P. Avouris, *Physical Review B* **68** (2003).
26. S. Heinze *et al.*, *Phys. Rev. Lett.* **89** (2002).
27. S. Heinze, J. Tersoff, P. Avouris, in *Introducing Molecular Electronics* G. Cuniberti, Ed. (Springer, Berlin, Berlin, 2005), vol. 680.
28. Z. Chen, J. Appenzeller, J. Knoch, Y. Lim, P. Avouris, *Nano Lett.* **5**, 1497 (2005).
29. A. Javey *et al.*, *Nano Letters* **4**, 447 (2004).
30. V. Perebeinos, J. Tersoff, P. Avouris, *Physical Review Letters* **94**, 086802 (2005).
31. A. Javey, P. F. Qi, Q. Wang, H. J. Dai, *Proc. Natl. Acad. Sci. U. S. A.* **101**, 13408 (2004).
32. Y. M. Lin, J. Appenzeller, J. Knoch, P. Avouris, *IEEE Transact. Nanotech.* (2005).
33. S. J. Tans, A. R. M. Verschueren, C. Dekker, *Nature* **393**, 49 (1998).

34. R. Martel, T. Schmidt, H. R. Shea, T. Hertel, P. Avouris, *Appl. Phys. Lett.* **73**, 2447 (1998).
35. M. Bockrath *et al.*, *Phys. Rev. B* **61**, 10606 (2000).
36. P. G. Collins, K. Bradley, M. Ishigami, A. Zettl, *Science* **287**, 1801 (2000).
37. K. Bradley *et al.*, *Phys. Rev. Lett.* **85**, 4361 (2000).
38. R. Martel *et al.*, *Phys. Rev. Lett.* **87**, art. no. (2001).
39. V. Derycke, R. Martel, J. Appenzeller, P. Avouris, *Appl. Phys. Lett.* **80**, 2773 (2002).
40. J. Kong *et al.*, *Science* **287**, 622 (2000).
41. T. Ando, *Journal of the Physical Society of Japan* **66**, 1066 (1997).
42. H. Sakai, H. Suzuura, T. Ando, *Journal of the Physical Society of Japan* **72**, 1698 (2003).
43. C. D. Spataru, S. Ismail-Beigi, L. X. Benedict, S. G. Louie, *Physical Review Letters* **92** (2004).
44. R. Egger, *Physical Review Letters* **83**, 5547 (1999).
45. C. Kane, L. Balents, M. P. A. Fisher, *Physical Review Letters* **79**, 5086 (1997).
46. M. Bockrath *et al.*, *Nature* **397**, 598 (1999).
47. H. W. C. Postma, M. de Jonge, Z. Yao, C. Dekker, *Physical Review B* **62**, 10653 (2000).
48. H. Ishii *et al.*, *Nature* **426**, 540 (2003).
49. R. Loudon, *Am. J. Phys.* **27**, 649 (1959).
50. V. Perebeinos, J. Tersoff, P. Avouris, *Physical Review Letters* **92**, 257402 (2004).
51. F. Wang, G. Dukovic, L. E. Brus, T. F. Heinz, *Science* **308**, 838 (2005).
52. J. A. Misewich *et al.*, *Science* **300**, 783 (2003).
53. M. Freitag *et al.*, *Phys. Rev. Lett.* **93**, 076803 (2004).
54. M. Freitag, Y. Martin, J. A. Misewich, R. Martel, P. Avouris, *Nano Lett.* **3**, 1067 (2003).
55. T. W. Odom, H. Jin-Lin, P. Kim, C. M. Lieber, *Nature* **391**, 62 (1998).
56. J. W. G. Wildoer, L. C. Venema, A. G. Rinzler, R. E. Smalley, C. Dekker, *Nature* **391**, 59 (1998).
57. R. H. Baughman *et al.*, *Science* **284**, 1340 (1999).
58. K. H. An *et al.*, *Advanced Materials* **13**, 497 (2001).
59. E. S. Snow, J. P. Novak, P. M. Campbell, D. Park, *Applied Physics Letters* **82**, 2145 (2003).
60. E. S. Snow *et al.*, *Journal of Vacuum Science & Technology B* **22**, 1990 (2004).
61. K. Bradley, J. C. P. Gabriel, G. Gruner, *Nano Lett.* **3**, 1353 (2003).
62. E. Artukovic, M. Kaempgen, D. S. Hecht, S. Roth, G. Gruner, *Nano Letters* **5**, 757 (2005).
63. P. C. Collins, M. S. Arnold, P. Avouris, *Science* **292**, 706 (2001).
64. M. Kruger, I. Widmer, T. Nussbaumer, M. Buitelaa, C. Schonenberger, *New Journal of Physics* **5** (2003).
65. A. Bachtold *et al.*, *Nature* **397**, 673 (1999).
66. A. Bachtold *et al.*, *Phys. Rev. Lett.* **87**, 6801 (2001).
67. P. G. Collins, P. Avouris, *Appl. Phys. A-Mater. Sci. Process.* **74**, 329 (2002).
68. S. Frank, P. Poncharal, Z. L. Wang, W. A. de Heer, *Science* **280**, 1744 (1998).

69. P. Poncharal, C. Berger, Y. Zi, Z. L. Wang, W. A. d. Heer, *J. Phys. Chem. B* **106**, 12104 (2002).
70. T. W. Ebbesen *et al.*, *Nature* **382**, 54 (1996).
71. J. Cumings, W. Mickelson, A. Zettl, *Solid State Commun.* **126**, 359 (2003).
72. S. Banerjee, T. Hemraj-Benny, S. S. Wong, *Adv. Mater.* **17**, 17 (2005).
73. M. J. Biercuk *et al.*, *Appl. Phys. Lett.* **80**, 2767 (2002).
74. R. H. Baughman, A. A. Zakhidov, W. A. d. Heer, *Science* **297**, 787 (2002).
75. C. S. Du, J. Yeh, N. Pan, *Nanotechnology* **16**, 350 (2005).
76. G. T. Wu *et al.*, *J. Electrochem. Soc.* **146**, 1696 (1999).
77. P. Kim, C. M. Lieber, *Science* **286**, 2148 (1999).
78. M. M. J. Treacy, T. W. Ebbesen, J. M. Gibson, *Nature* **381**, 678 (1996).
79. P. Poncharal, Z. L. Wang, D. Ugarte, W. A. de Heer, *Science* **283**, 1513 (1999).
80. T. Rueckes *et al.*, *Science* **289**, 94 (2000).
81. J. M. Bonard, H. Kind, T. Stockli, L. A. Nilsson, *Solid-State Electron.* **45**, 893 (2001).
82. G. Z. Yue *et al.*, *App. Phys. Lett.* **81**, 355 (2002).
83. G. U. Sumanasekera, C. K. W. Adu, S. Fang, P. C. Eklund, *Phys. Rev. Lett.* **85**, 1096 (2000).
84. A. Star, J. C. P. Gabriel, K. Bradley, G. Gruner, *Nano Lett.* **3**, 459 (2003).
85. M. S. Dresselhaus, P. Avouris, in *Carbon Nanotubes* M. S. Dresselhaus, P. Avouris, Eds. (Springer-Verlag Berlin, Berlin, 2001), vol. 80, pp. 1-9.
86. Y.-M. Lin, P. Avouris, *Electron Device Lett.*, in press (2005).
87. X. H. Qiu, M. Freitag, V. Perebeinos, P. Avouris, *Nano Lett.* **5**, 749 (2005).
88. A. Star, T. R. Han, V. Joshi, J. C. P. Gabriel, G. Gruner, *Advanced Materials* **16**, 2049 (2004).